

# Morphology and lattice distortions of nitrided iron and iron–chromium alloys and steels

E. J. MITTEMEIJER, A. B. P. VOGELS, P. J. VAN DER SCHAAF  
*Laboratory of Metallurgy, Delft University of Technology, Rotterdamseweg 137,  
2628 AL Delft, The Netherlands*

Specimens prepared from iron, iron–chromium alloys (0 to 4 wt% Cr) and commercial steels (C45, 41Cr4, 15CrNi6 and 24CrMo13) were powder nitrided at 818 K for 0.25 to 32 h. After cooling to room temperature the resulting morphology, lattice distortions and compositional variations were determined by X-ray diffraction analysis, metallographic methods and electron microprobe analysis. In the diffusion zone of iron and iron–chromium (0.54 wt% Cr),  $\alpha''$ -(Fe<sub>16</sub>N<sub>2</sub>)- and  $\gamma'$ -(Fe<sub>4</sub>N)-nitrides were observed, whereas specimens of the iron–chromium alloys with a higher chromium content showed a finely dispersed submicroscopical precipitation of CrN in the matrix and precipitates of Cr<sub>2</sub>N at the grain boundaries. With increasing nitriding times for the iron–chromium alloy with the highest chromium content (3.82 wt% Cr) a discontinuous precipitation starting from the grain boundaries occurred. For the first time recrystallization phenomena in the diffusion zone were observed, indicating that the inward diffusion of nitrogen introduces large lattice distortions. Large distortions were determined from X-ray diffraction line shift and line broadening respectively. The behaviour of macro- and micro-strain as a function of nitriding time was interpreted in terms of the volume changes caused by nitriding and subsequent precipitation. The residual surface stresses were calculated from the macrostrains applying the Voigt–Reuss-mean model. The experimentally determined ratio of the macrostrains in the (100) and the (110) directions was in good agreement with the value predicted from the model. The corresponding ratio of the microstrains was significantly larger than this theoretical prediction, which can be attributed to precipitates growing along (100) planes in the matrix (such as  $\alpha''$ -nitride and CrN). In contrast with the macrostrain, a strong relation was found between the microstrain and the chromium content of the specimen.

## 1. Introduction

At present, nitrided steels have many technologically important applications [1]. Nitriding yields the best fatigue resistance of any surface treatment and, in particular after nitrocarburizing, good tribological and anticorrosion properties. However, a considerable gap exists between the achievement of successful application and understanding. It is felt that the fatigue properties are principally determined by the lattice distortions in the nitrided zone, but detailed knowledge on the

behaviour on nitriding of the macro- and micro-strains is still lacking.

In view of the above, the present investigation was initiated to produce a description of the lattice distortions due to nitriding. Pure iron, iron–chromium alloys (containing up to 4 wt% Cr) and several steels (C45, 41Cr4, 15CrNi6 and 24CrMo13 with a chromium content in the range 0 to 4 wt% Cr) were investigated, since chromium is the main alloying element in many steels developed for nitriding.

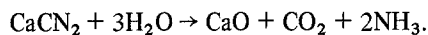
X-ray diffraction methods (macro- and micro-strain; phase identification), metallographic methods (optical microscopy; hardness measurement) and electron microprobe analysis (composition variations) were employed.

## 2. Experimental procedure

### 2.1. Specimen preparation

Specimens in the form of discs (diameter about 20 mm; thickness about 2 mm) were prepared from iron with residual elements at low levels (total amount < 0.02 wt%), also iron–chromium alloys (containing 0.54, 1.06, 2.00 and 3.82 wt% Cr) and several quenched and tempered steels (austenitized (2 h, 840° C); water quenched; tempered (2 h, 600° C); air cooled). For compositions, see Table I.

After mechanically polishing (final stage 1 μm diamond), nitriding was carried out in "Effge" powder (Goering & Co), in a closed box (kitted with "Lenit-Härtschutz", Soth) in a furnace at 818 K (± 2 K). In this method [2] the powder CaCN<sub>2</sub> (calciumcyanamide) reacts with H<sub>2</sub>O, delivered at the nitriding temperature by an enclosed activator, according to



Nitrogen is produced by dissociation of NH<sub>3</sub> and carbon is produced according to the Boudouard equilibrium. The method can be compared with other nitrocarburizing methods, e.g. salt-bath nitriding [3]. A calibrated Pt/PtRh (13% Rh) thermocouple placed within the box was used to indicate the start of nitriding. Annealing times in the range 0.25 to 32 h were employed. After nitriding the boxes were air-cooled.

### 2.2. Metallography

Optical microscopy was performed with a Neophot-2 (Carl Zeiss, Jena). Polarized light was applied to differentiate between optically isotropic and optically anisotropic phases. To enhance contrast physical etching by a vapour deposited interference filter was used.

The microhardness profiles were determined applying a Vickers micro-hardness tester, according to Hanemann, adapted to the Neophot-2 microscope (applied load 4.5 g).

### 2.3. Microprobe analysis

Applying ARL and Jeol electron microprobes, the nitrogen and carbon concentrations were determined as a function of the distance below the surface from the characteristic NKα and CKα lines respectively. To minimize contamination, a plate cooled by liquid nitrogen was installed near the specimen. Moreover, in the case of the carbon measurements an oxygen jet was aimed at the spot investigated on the specimen.

For quantitative results the measured intensities have to be related to the intensities measured from standard specimens. In the literature diverging or only qualitative results have been reported [4–6] which may be due to a lack of good standards (especially for nitrogen [6]). In the present work an Fe<sub>3</sub>C standard was employed for the carbon analysis. For the nitrogen analysis a γ'-Fe<sub>4</sub>N standard was prepared by gas-nitriding, as described elsewhere [7], under appropriate conditions [8].

### 2.4. Diffractometry

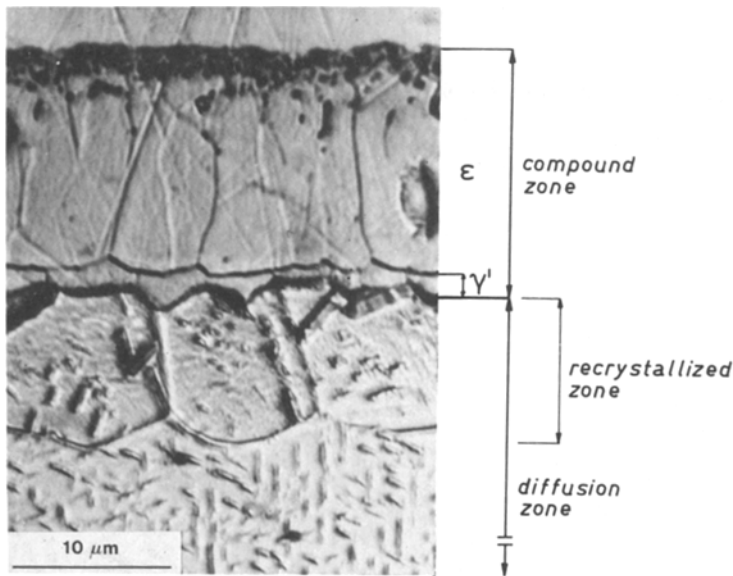
For the purpose of phase identification, fast scans over the range 25 to 130° 2θ were made (scan-speed about 2° 2θ min<sup>-1</sup>) employing a Siemens type F ω-diffractometer equipped with a graphite monochromator in the diffracted beam and using CoKα radiation.

For the determination of the macrostrain (from the line shift) and the microstrain (from the line broadening) the {200} and {220} line profiles of the iron-matrix were recorded with low scan-speeds (usually about 0.1° 2θ min<sup>-1</sup>) to obtain sufficient counting accuracy. Large portions of the background at both sides of the peak were recorded. The background was interpolated linearly between both extremities. The α<sub>2</sub> component was eliminated by computation [9]. For the elimination of the broadening due to the instrumental aberrations

TABLE I Compositions of steels

| Steel    | Composition (wt%) |      |      |       |       |      |      |      |
|----------|-------------------|------|------|-------|-------|------|------|------|
|          | C                 | Si   | Mn   | P     | S     | Cr   | Ni   | Mo   |
| C45      | 0.45              | 0.40 | 0.80 | 0.035 | 0.025 | —    | —    | —    |
| 41Cr4    | 0.41              | 0.25 | 0.70 | 0.035 | 0.035 | 1.05 | —    | —    |
| 15CrNi6  | 0.15              | 0.25 | 0.40 | 0.035 | 0.035 | 1.55 | 1.55 | —    |
| 24CrMo13 | 0.24              | 0.35 | 0.59 | 0.050 | 0.050 | 3.20 | 0.40 | 0.61 |

Figure 1 Cross-section of a specimen of iron nitrided for 8 h at 818 K (oblique incidence; X oil immersion).



and the X-ray spectrum used, the corresponding line profiles were recorded from standard specimens, chemically identical to the specimens to be investigated, which were subjected to the same (heat) treatment but with the exclusion of nitriding.

### 3. Morphology

A cross-section of a nitrided iron specimen is shown in Fig. 1. The nitrided zone is usually subdivided into the compound layer, directly below the surface, and the diffusion zone [3].

#### 3.1. The compound layer

X-ray diffraction analysis indicated the presence of  $\epsilon$ - $\text{Fe}_{2-3}\text{N}(\text{C})$ ,  $\gamma'$ - $\text{Fe}_4\text{N}$  and  $\text{Fe}_3\text{O}_4$  (a very thin layer at the surface). Using polarized light it was possible to distinguish between  $\epsilon$ - (optically anisotropic) and  $\gamma'$ - (optically isotropic) nitride (Fig. 2).

An example of the microprobe analysis of a nitrided steel is shown in Fig. 3. In the nitrogen concentration profile the  $\epsilon$ - and  $\gamma'$ -nitride regions can be observed. From the carbon concentration profile it follows that carbon enrichment is observed only in the  $\epsilon$ -layer, which, as noted in [10], improves the resistance to scuffing and wear. The ranges observed for the nitrogen and carbon concentrations in the surface regions of the powder nitrided steels of this study (Fig. 3) correspond with values obtained with salt-bath nitriding [3] and gaseous nitrocarburizing [11]. Further, applying an Auger depth profiling technique, it was

recently shown [12] that no carbon could be detected in the surface region of powder nitrided iron. In accordance with [13], it is concluded that the main influence of the presence of carbon in the nitriding atmosphere consists of improved nitriding kinetics.

Near the surface, the  $\epsilon$ -layer is usually porous (Fig. 1). For the nucleation of the pores it has been suggested [14] that, due to the very high pressure of molecular nitrogen in equilibrium with the nitrogen in the  $\epsilon$ -phase, nitrogen atoms associated with dislocations (Cottrell-atmospheres) combine into nitrogen molecules which may be stable in spite of the local compressive stress. This idea implies that the pores will be found preferentially near the surface where the nitrogen concentration is largest (Fig. 3), as is observed (Fig. 1). The presence of pores also implies a large surface area available for oxidation. Some metallographic indications were obtained for the presence of oxides in the pores.

#### 3.2. The diffusion zone

In the iron specimens, both the metastable  $\alpha''$ - $(\text{Fe}_{16}\text{N}_2)$ -nitride [15] and the equilibrium  $\gamma'$ - $(\text{Fe}_4\text{N})$ -nitride were observed (small and large precipitates respectively in Fig. 4). These precipitates formed during cooling to room temperature from the supersaturated interstitial solid solution of nitrogen in iron.

On nitriding, no change in carbon concentration was observed in the diffusion zones of the nitrided

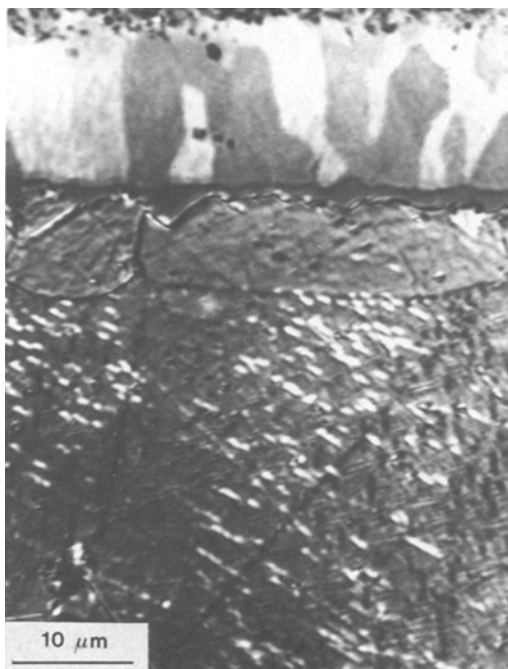


**Figure 2** Cross-section of a specimen of iron nitrided for 8 h at 818 K (polarized light, quartz compensator  $1/8\lambda$ ; oil immersion; vapour deposited ZnTe interference filter of optical thickness of  $\frac{1}{4}\lambda$ ;  $\lambda = 546$  nm). The  $\epsilon$ -layer is light (optically anisotropic) and the different grains can be distinguished, whereas the  $\gamma'$ -layer is dark (optically isotropic). In the diffusion zone the light precipitates are  $\alpha''$ -nitride (optically anisotropic). Note that practically no  $\alpha''$ -precipitates are seen in the recrystallized zone.

steels and no carbon could be detected in the diffusion zone of nitrided iron (see also Section 3.1.).

To our knowledge, recrystallization phenomena in the diffusion zone of nitrided iron, directly below the compound layer, were observed for the first time (Fig. 1). The zone of small crystallites observed was absent before nitriding. It might be argued that specimen preparation caused deformation in the surface of the specimen, thus inducing recrystallization. The only possible deformation before nitriding was due to the mechanical polishing treatment (final stage:  $1\mu\text{m}$  diamond). However, the diffraction lines observed after polishing before nitriding were sharp, indicating negligible deformation in the surface region of the specimen.

The recrystallization phenomena can be understood as follows. On nitriding, large lattice distortions arise from the inward diffusion of nitrogen. It has recently been shown [7] that during nitriding many dislocations are created to accommodate the misfit introduced by the nitrogen concentration profile. At the nitriding temperature these

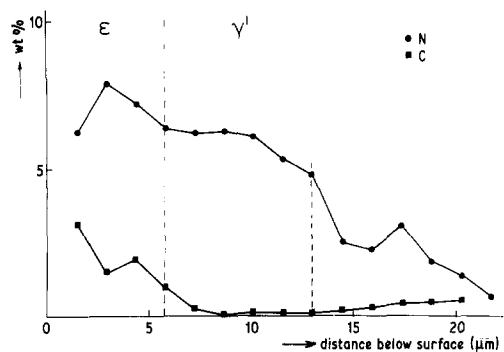


**Figure 3** Nitrogen and carbon concentrations as a function of the distance below the surface for a C45 specimen nitrided for 16 h at 818 K as determined by electron microprobe analysis. The regions of  $\epsilon$ - and  $\gamma'$ -nitride in the compound zone have been indicated. The nitrogen concentration in the diffusion zone directly below the  $\gamma'$ -nitride region is larger than the value which may be expected from phase equilibrium data [23]. This is caused by the offshoots from the  $\gamma'$ -region into the diffusion zone (spot size microprobe  $\approx 1\mu\text{m}$ ).

dislocations may form dislocation walls [16]. This polygonization process may in itself lead to recrystallization (via subgrain-boundary formation) or independent simultaneous recrystallization processes may occur, as has been observed in thin film bimetallic diffusion couples [17].

The  $\alpha''$ -nitrides nucleate on the diffusion-induced dislocations [7]. Therefore the notion of a recrystallized zone, where naturally a low dislocation density is expected, is supported by a very low number of  $\alpha''$ -nitrides in this zone (Fig. 2).

In agreement with the above model for recrystallization in nitrided iron, recrystallization

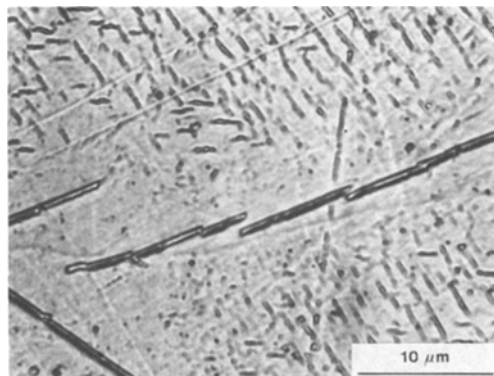


**Figure 4** Diffusion zone of a specimen of iron nitrided for 8 h at 818 K (oblique incidence; oil immersion). The small precipitates are  $\alpha''(\text{Fe}_{16}\text{N}_2)$ -nitride, the large precipitates are  $\gamma'(\text{Fe}_4\text{N})$ -nitride.

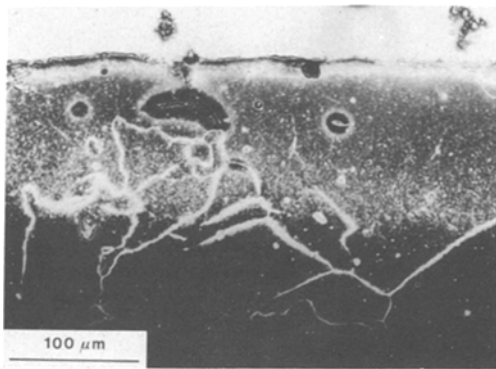


**Figure 5** Cross-section of a specimen of iron–chromium (3.82 wt% Cr) nitrided for 8 h at 818 K (monochromatic light (530 nm); bright field; vapour deposited ZnTe interference filter of optical thickness of  $\frac{1}{4}\lambda$ ;  $\lambda = 546$  nm). The bright, light precipitates along the grain boundaries are  $\text{Cr}_2\text{N}$ -precipitates. The light band corresponds to the diffusion zone matrix with submicroscopical finely-dispersed CrN. Note that  $\text{Cr}_2\text{N}$  is already present at grain boundaries which, at that stage, is mainly unnitrided material, which indicates that grain boundary is much faster than volume diffusion.

is observed directly below the compound layer where the nitrogen concentration gradient, and consequently the lattice distortion, will be largest. Differences in the degree of homogenization before and after the migrating recrystallization front may also add to the driving force for this process (difference in chemical Gibbs free energy). It is further remarked that migrating boundaries themselves enhance the homogenization process as the contribution of grain-boundary diffusion becomes more important [17].

X-ray diffraction and metallographic analyses of the nitrided iron–chromium alloy containing 0.54 wt% Cr showed the same nitrides as observed in nitrided iron. With a larger chromium content (1.06 wt% Cr), no precipitates were observed by microscopy in the grains of the diffusion zone. However, X-ray diffraction analysis indicated the presence of CrN. Hence it is concluded that, on nitriding, *submicroscopical* CrN-precipitates are formed. Further precipitates along grain boundaries were observed (Fig. 5). The use of polarized light (CrN is optically isotropic;  $\text{Cr}_2\text{N}$  is optically anisotropic), suggests that these precipitates are  $\text{Cr}_2\text{N}$ .

The chromium nitrides, in contrast with the iron nitrides discussed above, precipitate at the nitriding temperature.

With increasing nitriding times for the iron–

chromium alloy containing 3.82 wt% Cr, a discontinuous precipitation, starting from the grain boundaries, occurred. This process continued until the surface layer of the matrix was completely transformed (Fig. 6). X-ray diffraction analysis suggested the conversion  $\text{CrN} \rightarrow \text{Cr}_2\text{N}$ : a ridge of intensity was observed in the range where the  $\{2\ 1\ 1\}$ - $\text{CoK}\alpha$ - $\text{Cr}_2\text{N}$  reflection is expected (iron can be included in the  $\text{Cr}_2\text{N}$  lattice). Below the surface layer of the matrix, optical reflectivity measurements indicated a nitrided layer, presumably containing submicroscopical CrN precipitates.

The driving force for the conversion  $\text{CrN} \rightarrow \text{Cr}_2\text{N}$  may be due to the significant reduction in interfacial energy, as the CrN-precipitates are finely dispersed (submicroscopical) in contrast with the  $\text{Cr}_2\text{N}$ -precipitates, and also the  $\text{Cr}_2\text{N}$  can be stabilized in the surface region by the compressive residual stress (see Section 5.1.) since its specific volume is considerably less than that of CrN (see Fig. 7b and Section 4). In the absence of these factors it can be shown from standard thermodynamic data [18] that at 818 K, CrN is a more stable nitride than  $\text{Cr}_2\text{N}$ .

Mortimer, Grieveson and Jack [19] have previously studied precipitation in iron–chromium alloys. For their nitriding conditions, they observed, in iron–chromium alloys containing more than 5 wt% Cr, that nitriding below 600° C produced growth from the grain boundaries. They identified the new precipitates as CrN instead of  $\text{Cr}_2\text{N}$ . Further work is needed to clarify this point.

Jack [20] has proposed that precipitation of nitrides in ferritic alloys proceeds through a mixed substitutional–interstitial solute–atom cluster (Guinier–Preston-zone) stage and an intermediate precipitate (of the type  $\alpha''\text{-Fe}_{16}\text{N}_2$ ) stage. This has not been confirmed for iron–chromium alloys [19] but indications for an intermediate precipitate stage have been obtained on nitriding pure chromium [21].

### 3.3. Microhardness profile

Obviously the porous zone corresponds to low hardness. In the compound layer the  $\gamma'$ -nitride shows the greatest hardness.

In the nitrided specimens of iron, iron–chromium alloy with 0.54 wt% Cr and C45, the hardness in the diffusion zone gradually decreased with increasing distances from the surface thus reflecting the (at the nitriding temperature interstitially solved) nitrogen concentration profile,

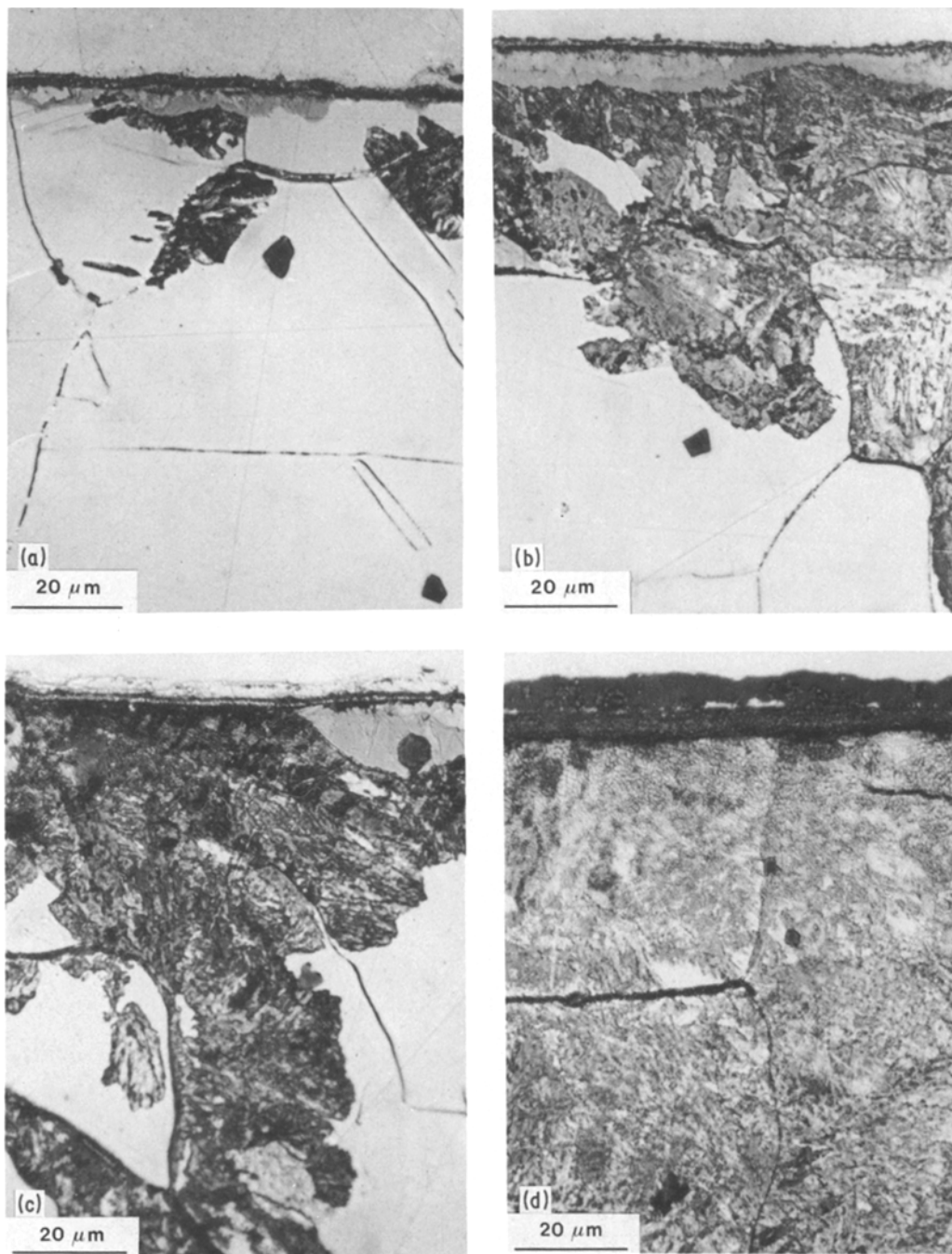


**Figure 6** The cross-sections of specimens of iron–chromium (3.82 wt% Cr) nitrided for (a) 4 h, (b) 8 h, (c) 16 h and (d) 32 h, respectively at 818 K (oblique incidence; oil immersion). With increasing nitriding times a discontinuous precipitation takes place, starting from the grain boundaries.

now in the form of iron nitrides which precipitated during cooling to room temperature. In the other specimens, the precipitates were formed at the nitriding temperature. Then the total amount of alloying element can be precipitated as nitride and

thus a constant hardness level will be present in the upper part of the diffusion zone (see also Section 5.2, and Fig. 8). As expected, the constant hardness level increased with the chromium content of the alloy (1.06 wt% Cr: 605 HV; 2.00 wt%

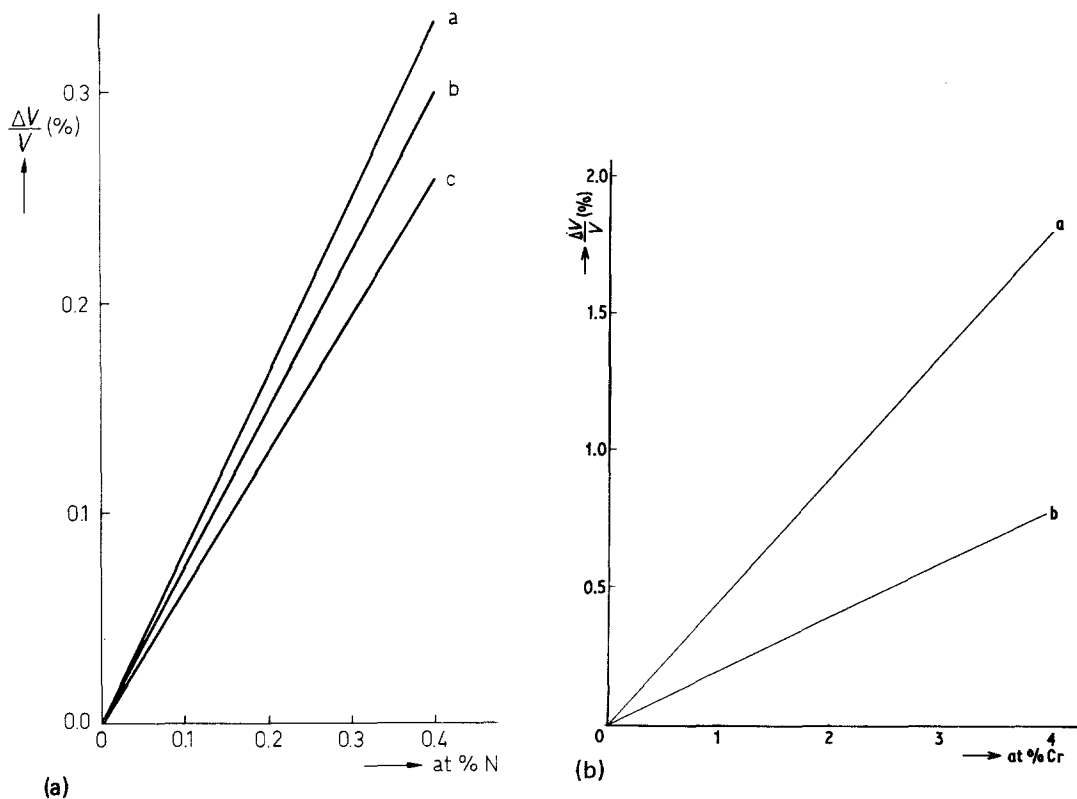


Figure 7(a) The relative volume change due to interstitially solved nitrogen in the iron matrix as compared to pure iron, as a function of the atomic percentage nitrogen solved (line a), and the relative volume changes if all nitrogen is precipitated as  $\alpha''$ - or  $\gamma'$ -nitride (lines b and c respectively). (b) The relative volume changes due to precipitation of  $\text{Cr}_2\text{N}$  and  $\text{Cr}_2\text{N}$  compared with the substitutional iron-chromium solid solution, as a function of alloy composition (lines a and b respectively).

Cr: 780 HV; 3.82 wt% Cr: 930 HV, see also below). Iron-chromium specimens containing significant amounts of both submicroscopical  $\text{CrN}$  and discontinuous precipitate showed a marked difference in hardness between the matrix and the transformed region, the matrix being considerably harder (matrix: about 930 HV; transformed region: about 540 HV).

#### 4. Volume changes

On nitriding, the outer shell of the specimen is expanded compared with the core of the specimen. As a result, a macrostrain, corresponding to a compressive residual surface stress, will be invoked in the diffusion zone. Further precipitation phenomena may induce local variations in the lattice parameter (microstrains). Therefore, a relation exists between the volume changes occurring on nitriding and the lattice distortions.

In Fig. 7a the relative volume change due to nitrogen solved interstitially in the iron matrix, as

compared to pure iron, is shown as a function of the atomic percentage nitrogen solved (line a). Lattice parameter data for this calculation were taken from [22]. Also, the relative volume changes are shown in the case of all the nitrogen being precipitated as  $\alpha''$ - or  $\gamma'$ -nitride (lines b and c respectively). Lattice parameter data for these calculations were taken from [23]. According to the literature [24], the nitrogen content of iron nitrided at 818 K is 0.27 to 0.34 at %N. It then follows from Fig. 7a that a volume change of the order of 0.2% occurs on nitriding. It is seen that only minor volume changes occur if  $\alpha''$ - and  $\gamma'$ -nitrides precipitate from a supersaturated solid solution of nitrogen in iron. Therefore, it may be concluded that the macrostrain due to nitriding does not change significantly when precipitation of iron nitrides occurs from the nitrogen-iron solid solution (in particular for ageing experiments at room temperature where only  $\gamma'$ -precipitates form [7]). In addition, it follows from the calculations that the

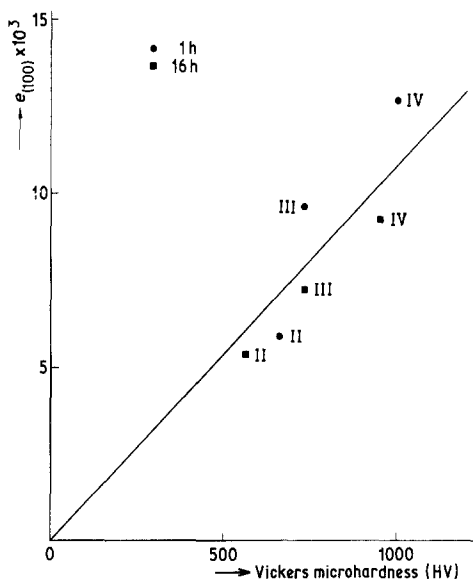


Figure 8 The microstrain in the (110) direction perpendicular to the surface against the constant hardness level in the upper part of the diffusion zone for nitrided (1 h and 16 h, respectively, at 818 K) specimens of several steels (II = 41Cr4; III = 15CrNi6; IV = 24CrMo13).

misfit between the bottom of the compound zone ( $\gamma'$ -layer) and the top of the diffusion zone (nitrided iron) is about 5.3% (for nitriding at 818 K). This misfit may be the reason for the cracks observed sometimes in the interface between compound and diffusion zones. The misfit between the bottom of the  $\epsilon$ -layer in the compound layer, corresponding to  $\epsilon\text{-Fe}_3\text{N}(\text{C})$ , and the  $\gamma'$ -layer, is about 0.1%. Therefore the  $\epsilon$ - and  $\gamma'$ -layers will remain closely bound.

The volume changes occurring on nitriding iron–chromium alloys can be calculated analogously from lattice parameter data given in [25]. In Fig. 7b the relative volume changes due to precipitation of CrN and  $\text{Cr}_2\text{N}$ , as compared to the substitutional iron–chromium solid solution, are shown as a function of alloy composition (lines a and b respectively). If all chromium present is precipitated as nitride (in this investigation this has been observed for chromium contents of 1.06 wt% and larger; see Section 3), then it can be concluded that much larger volume effects (and hence lattice distortions) can be expected than when nitriding iron (see Fig. 7a and b): volume changes in the range 0.5 to 2% occur.

## 5. Lattice distortions

Two kinds of lattice distortions in the diffusion zone are distinguished.

(i) A macrostrain is introduced because the lattice dilatation by nitriding in the outer shell of the specimen is counterbalanced by a compressive residual surface stress. The macrostrain corresponds to an (average) change of the lattice parameter and can be derived from measurement of the X-ray diffraction line shift.

(ii) Microstrains are introduced because nitride precipitates bring about local fluctuations of the lattice parameter around the (new) average lattice parameter. A measure for the average microstrain can be derived from the X-ray diffraction line broadening data.

It is noted that the X-ray diffraction method only allows the determination of *elastic* strains. Further, the information obtained is only an average over the part of the diffusion zone directly below the compound layer. The compound layer was not removed from the specimens. This had the advantage that possible relaxation effects were avoided. It could further be shown that the line shift which resulted from this geometry, because the axis of the diffractometer did not lie in the surface of the iron matrix, was negligible compared with the effects observed.

### 5.1. Macrostrain

The macrostrain,  $\epsilon$ , perpendicular to the surface, as derived from the  $\{200\}$  and  $\{220\}$  X-ray diffraction peak positions for iron matrix crystals with a  $\{100\}$  and a  $\{110\}$  plane respectively parallel to the surface, is shown as a function of nitriding time in Fig. 9 for specimens of iron, C45 and an iron–chromium alloy (3.82 wt% Cr). For iron and C45, the spacing changes have been calculated relative to the peak positions of unnitrided iron and unnitrided C45 respectively. For the iron–chromium alloy, the spacing changes have been calculated relative to the peak position of unnitrided iron instead of unnitrided iron–chromium because all chromium is precipitated (after nitriding for 1 h a constant hardness level is observed in the upper part of the diffusion zone).

From Fig. 9 it is seen that for the three types of specimen the macrostrains are relatively large at small nitriding times ( $\approx 1$  h). With increasing nitriding times the macrostrains diminish and become effectively zero for iron and iron–chromium, while a constant level is reached with C45. Although at present these phenomena are not completely understood, the following remarks can be made.

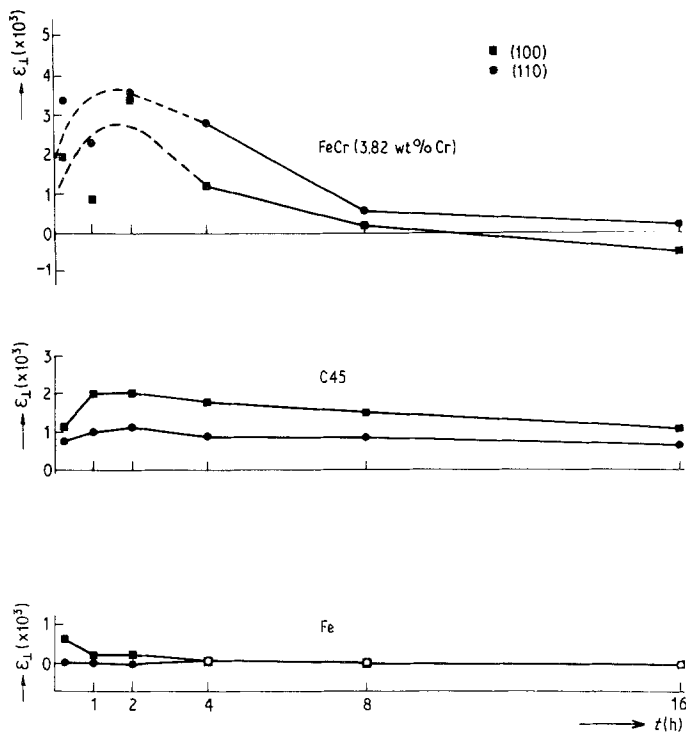


Figure 9 The macrostrains  $\epsilon$  perpendicular to the surface for iron-matrix crystals with a  $\{100\}$  and a  $\{110\}$  plane, respectively, parallel to the surface, as a function of nitriding time (at 818 K) for specimens of iron, C45 and an iron-chromium alloy (3.82 wt% Cr).

Until the diffusion zones become saturated with nitrogen, the macrostrains will increase due to volume expansion as discussed in Section 4. As expected (Fig. 7a and b), the macrostrain will be larger for the iron-chromium alloy than for iron. The lowering of the macrostrain of the iron-chromium alloy (3.82 wt% Cr) for larger nitriding times may be due to the occurrence of discontinuous precipitates; note that a possible conversion  $\text{CrN} \rightarrow \text{Cr}_2\text{N}$  is accompanied by a volume contraction, as compared to the volume at an early stage of nitriding (Fig. 7b). Obviously, after homogeneously nitriding, the constraint by the non-nitrided core and the corresponding macrostrain will be absent. However a negligible macrostrain in pure iron is observed (Fig. 9) long before the specimen could be nitrided homogeneously (as could be seen from the nitriding times applied and the diffusion coefficient of nitrogen in iron [26] and as was demonstrated by the microhardness profiles measured). At present, more detailed experiments are in progress with pure iron and iron-carbon alloys to investigate the diminishing macrostrain in pure iron (relation to diffusion generation of dislocations [7]) and the effect of cementite in the iron matrix. An experiment with a FeC (0.4 wt% C)-specimens (gas-nitrided for 4.5 h at 843 K and subsequently cooled to room tem-

perature) showed that in pearlite mainly  $\alpha''$ -nitrides were present whereas in ferrite both  $\alpha''$ - and  $\gamma'$ -nitrides were observed. According to Fig. 7a,  $\alpha''$ -nitrides imply a larger volume effect than  $\gamma'$ -nitrides. This can contribute to the occurrence of larger macro- and microstrains (see Section 5.2.) in C45 compared with pure iron.

Specimens of commercial steels also showed a decreasing macrostrain on prolonged nitriding (Table II). The effect appears to be independent of the nature of the nitriding process employed as very recently the same trend was observed after gaseous nitrocarburizing [27]. In view of the relation usually assumed between the fatigue resistance and the residual surface stress [28] this observation may be of practical importance; if the fatigue resistance is determined dominantly by the macrostrain (but see Section 5.2.) it may be suggested that short nitriding times should be preferred. However, experiments with a salt-bath nitrided steel did not show a reproducibly diminishing trend for the fatigue resistance with nitriding time [29].

Usually the macrostrains observed are larger in the (100) direction than in the (110) direction. This can be understood qualitatively as iron is weakest in the (100) direction. As an exception, specimens of the iron-chromium alloy (3.82 wt%

TABLE II The macrostrain  $\epsilon$  and the microstrain  $e$  in the direction perpendicular to the surface for iron-matrix crystallites with a  $\{100\}$  plane and a  $\{110\}$  plane, respectively, parallel to the surface, and the residual surface stress  $\sigma$  as calculated from the macrostrain using the Voigt–Reuss-mean model (Equation 1).

| Steel    | Nitriding time (h) | $\epsilon (\times 10^3)$ |     | $-\sigma$ (MPa) |      | $e (\times 10^3)$ |     |
|----------|--------------------|--------------------------|-----|-----------------|------|-------------------|-----|
|          |                    | 100                      | 110 | 100             | 110  | 100               | 110 |
| C45      | 1                  | 2.0                      | 1.0 | 490             | 390  | 2.4               | 1.4 |
|          | 16                 | 1.1                      | 0.7 | 270             | 280  | 2.1               | 1.2 |
| 41Cr4    | 1                  | 3.3                      | 1.7 | 810             | 670  | 5.9               | 3.1 |
|          | 16                 | 1.7                      | 1.5 | 420             | 590  | 5.4               | 2.4 |
| 15CrNi6  | 1                  | 5.6                      | 2.5 | 1380            | 990  | 9.7               | 5.5 |
|          | 16                 | 2.5                      | 1.9 | 620             | 750  | 7.3               | 3.4 |
| 24CrMo13 | 1                  | 2.4                      | 2.8 | 600             | 1110 | 12.8              | 6.1 |
|          | 16                 | 1.3                      | 1.4 | 330             | 560  | 9.3               | 4.1 |

Cr) unexpectedly show a macrostrain in the  $\{110\}$  direction larger than the one in the  $\{100\}$  direction (Fig. 9). This may be related to the discontinuous precipitation. For quantification the Voigt-Reuss-mean (Hill) model can be applied [30]. The residual surface stress  $\sigma$  follows (see also [7] and [13])

$$\sigma = \epsilon \left( s_{12} + sS + \frac{2s(s_{11} + 2s_{12}) + 5s_{12}s_{44}}{6s + 5s_{44}} \right)^{-1}, \quad (1)$$

where the symbols  $s_{ij}$  denote the elastic compliances,

$$s = s_{11} - s_{12} - \frac{1}{2}s_{44}$$

and

$$S = (h^2k^2 + h^2l^2 + k^2l^2)/(h^2 + k^2 + l^2)^2,$$

with  $h$ ,  $k$  and  $l$  as the Miller indices. Using elastic data for iron [32], it follows from Equation 1 that  $\epsilon_{100}/\epsilon_{110} = 1.6$  in good agreement with the experimental average  $\langle \epsilon_{100}/\epsilon_{110} \rangle = 1.5$  of Table II. In Table II the compressive residual surface stresses calculated according to Equation 1 are also presented. Compared with the literature data for the residual surface stress in steels nitrided in various ways [28], values obtained by powder nitriding for the residual surface stress in commercial steels are of the same order of magnitude.

## 5.2. Microstrain

From the analysis of the X-ray diffraction line broadening the (small) crystallite size and the lattice distortion (microstrain) can be determined.

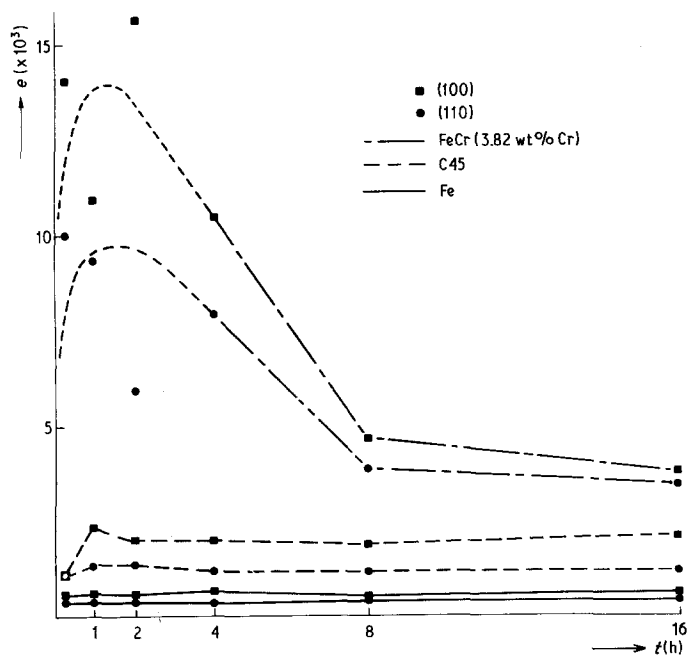


Figure 10 The microstrains  $e$  perpendicular to the surface and for iron-matrix crystals with a  $\{100\}$  and a  $\{110\}$  plane respectively parallel to the surface, as a function of nitriding time (at 818 K) for specimens of iron, C45 and an iron–chromium alloy (3.82 wt% Cr).

In this work, a recently developed single-line integral breadth method was applied (for details see [33], where also the validity of this technique for nitrided steels is justified experimentally).

The nitrided specimens gave rise to strain broadening only. In Fig. 10 the microstrain  $e$  perpendicular to the surface in iron matrix crystals with a  $\{100\}$  and a  $\{110\}$  plane respectively parallel to the surface is shown as a function of nitriding time for iron, C45 and iron–chromium (3.82 wt% Cr). The microstrains result from the precipitation processes. In iron and C45 iron nitrides and in iron–chromium, chromium nitrides are present in the diffusion zone (Section 3). As expected Fig. 7a and b) the largest microstrains are observed in the iron–chromium alloy. The lowering of the microstrain of the iron–chromium alloy (3.82 wt% Cr) may be due to the occurrence of discontinuous precipitation. Coarser precipitates usually cause smaller microstrains. With respect to the larger microstrain observed in C45 compared with pure iron, see also the discussion in Section 5.1.

The microstrains of the nitrided steels are summarized in Table II. The microstrains after nitriding for 1 h are somewhat larger than after 16 h nitriding. It may be expected that a relation exists between the constant hardness level in the upper part of the diffusion zone of the nitrided alloy (Section 3.3.) and the microstrain. From the present results an approximately linear dependence is found (Fig. 8).

As with the macrostrains, the distortions are larger in the  $(100)$  direction than in the  $(110)$  direction. It has been suggested for the case of cold-worked specimens that the Voigt–Reuss–mean (Hill) model should be applied to the microstrains also [34]. From Table II the experimental average  $\langle e_{100}/e_{110} \rangle = 2.0$  follows, which, in contrast to the macrostrain ratio, is significantly larger than the theoretical prediction of 1.6 (Section (5.1)). The large experimental value of  $\langle e_{100}/e_{110} \rangle$  can be understood because precipitates as  $\alpha''$ -nitride and CrN grow preferentially on  $\{100\}$  planes [19, 20], thus enhancing the strain anisotropy already implied by the inherent elastic behaviour of the iron matrix.

In contrast with the macrostrains, a strong relation is observed between microstrain and chromium content (Table II). It is also observed that the microstrains are up to 10 times larger than the macrostrains. It is concluded that the fatigue

properties are not fully characterized by the residual surface stress (as determined from the macrostrain) as is often done (e.g. [28]): the microstrain can be at least equally important.

## Acknowledgements

We are indebted to Professor B. M. Korevaar for stimulating discussions. We also benefitted by a helpful discussion with Dr. H. Kunst (Degussa, BRD). Dr. Ir. R. Delhez and Professor B. M. Korevaar read the manuscript critically. Dr. Ir. Th. H. de Keijser and Ing. N. M. van der Pers provided X-ray diffraction facilities. Mr. P. F. Colijn and Ir. D. Schalkoord performed optical microscopy and electron microprobe analyses, respectively.

## References

1. Source Book on Nitriding, (ASM, Metals Park, Ohio, 1977).
2. P. BIRK, *Microtechnic* **24** (1970) 277.
3. T. BELL, *Heat Treatment of Metals* **2** (1975) 39.
4. J. ZYŠK, *Härterei-Tech. Mitt.* **31** (1976) 137.
5. K. SACHS and D. B. CLAYTON, *Heat Treatment of Metals* **6** (1979) 29.
6. O. SCHAABER and H. VETTERS, *Härterei-Tech. Mitt.* **33** (1978) 305.
7. E. J. MITTEMEIJER, A. B. P. VOGELS and P. J. VAN DER SCHAAF, *Scripta Met.* **14** (1980) 411.
8. E. LEHRER, *Z. Electrochem.* **36** (1930) 383.
9. R. DELHEZ and E. J. MITTEMEIJER, *J. Appl. Cryst.* **8** (1975) 609.
10. B. PRENOSIL, *Härterei-Tech. Mitt.* **20** (1965) 41.
11. C. DAWES, D. F. TRANTER and C. G. SMITH, *Met. Technol.* **6** (1979) 395.
12. W. H. KOOL, E. J. MITTEMEIJER and D. SCHALKKOORD, Proceedings of the 9th Conference on X-ray Optics and Microanalysis (ICXOM), Vol. 3, 1980, The Hague, The Netherlands, (Electron Microscopy Foundation, Heiden, 1980) p. 228.
13. C. DAWES and D. F. TRANTER, *Met. Technol.* **5** (1978) 278.
14. B. PRENOSIL, *Härterei-Techn. Mitt.* **28** (1973) 157.
15. K. H. JACK, *Proc. Roy. Soc.* **A208** (1951) 216.
16. A. M. BEERS and E. J. MITTEMEIJER, *Thin Solid Films* **48** (1978) 367.
17. E. J. MITTEMEIJER and A. M. BEERS, *ibid.* **65** (1980) 125.
18. I. BARIN and O. KNACKE, "Thermochemical properties of inorganic substances" (Springer Verlag, Berlin, 1973).
19. B. MORTIMER, P. GRIEVESON and K. H. JACK, *Scan. J. Metall.* **1** (1972) 203.
20. K. H. JACK, *Proc. Heat Treatment 1973* (The Metals Society, London, 1973) p. 39.
21. G. S. WOODS and A. BALL, *Phil. Mag.* **27** (1973) 785.
22. H. A. WRIEDT and L. ZWELL, *Trans. AIME* **224** (1962) 1242.

23. D. H. HACK and K. H. JACK, *Mater. Sci. Eng.* 11 (1973) 1.
24. M. HANSEN, "Constitution of Binary Alloys" 2nd edition (McGraw Hill, New York, 1958) p. 673.
25. W. B. PEARSON, "A Handbook of Lattice Spacings and Structures of Metals and Alloys" Vol. 1 (Pergamon Press, Oxford and New York, 1972) p. 982.
26. J. D. FAST and M. B. VERRIJP, *J. Iron Steel Inst.* 176 (1954) 24.
27. R. Th. FURNÉE and E. J. MITTEMEIJER, unpublished work (1980).
28. J. C. GREGORY, *Heat Treatment of Metals* 2 (1975) 55.
29. H. KUNST, private communication (1980).
30. R. HILL, *Proc. Phys. Soc. A*52 (1952) 349.
31. C. N. J. WAGNER, J. P. BOISSEAU and E. N. AQUA, *Trans. AIME* 233 (1965) 1280.
32. C. J. SMITHELS, "Metals Reference Book", 5th edition (Butterworth, London, 1976) p. 978.
33. Th. H. DE KEIJSER, J. I. LANGFORD, E. J. MITTEMEIJER and A. B. P. VOGELS, in preparation.
34. R. DELHEZ, Th. H. DE KEIJSER and E. J. MITTEMEIJER in "Accuracy in Powder Diffraction", edited by S. Block and C. R. Hubbard, National Bureau of Standards Special Publication 567 (1980) 213.

Received 8 February and accepted 5 June 1980.